



Quad 14 Gbps L-band VCSEL-based system for WDM migration of 4-lanes 56 Gbps optical data links

Estaran Tolosa, Jose Manuel; Rodes Lopez, Roberto; Pham, Tien Thang; Ortsiefer, Markus; Neumeyr, Christian; Roskopf, Jürgen; Tafur Monroy, Idelfonso

Published in:
Optics Express

Publication date:
2012

Document Version
Publisher's PDF, also known as Version of record

[Link back to DTU Orbit](#)

Citation (APA):
Estaran Tolosa, J. M., Rodes Lopez, R., Pham, T. T., Ortsiefer, M., Neumeyr, C., Roskopf, J., & Tafur Monroy, I. (2012). Quad 14 Gbps L-band VCSEL-based system for WDM migration of 4-lanes 56 Gbps optical data links. *Optics Express*, 20(27), 28524-28531.

General rights

Copyright and moral rights for the publications made accessible in the public portal are retained by the authors and/or other copyright owners and it is a condition of accessing publications that users recognise and abide by the legal requirements associated with these rights.

- Users may download and print one copy of any publication from the public portal for the purpose of private study or research.
- You may not further distribute the material or use it for any profit-making activity or commercial gain
- You may freely distribute the URL identifying the publication in the public portal

If you believe that this document breaches copyright please contact us providing details, and we will remove access to the work immediately and investigate your claim.

Quad 14 Gbps L-band VCSEL-based system for WDM migration of 4-lanes 56 Gbps optical data links

Jose Estaran,^{1,*} Roberto Rodes,¹ Tien Thang Pham,¹ Markus Ortsiefer,²
Christian Neumeyr,² Jürgen Roskopf,² and Idelfonso Tafur Monroy¹

¹DTU Fotonik, Department of Photonics Engineering, Technical University of Denmark, DK2800 Kgs. Lyngby, Denmark

²VERTILAS GmbH, Lichtenbergstr. 8, D-85748 Garching, Germany
jome@fotonik.dtu.dk

Abstract: We report on migrating multiple-lane link into an L-band VCSEL-based WDM system. Experimental validation achieves successful transmission over 10 km of SMF at 4x14Gbps. Inter-channel crosstalk penalty is observed to be less than 0.5 dB and a transmission penalty around 1 dB. The power budget margin ranges within 6 dB and 7 dB.

© 2012 Optical Society of America

OCIS codes: (060.0060) Fiber optics and optical communications; (200.4650) Optical interconnects.

References and links

1. H. Liu, C. F. Lam, and C. Johnson, "Scaling optical interconnects in datacenter networks opportunities and challenges for WDM," in *Proceedings of the 18th Annual Symposium on High Performance Interconnects*, 2010, 113 – 116.
 2. A. Vahdat, H. Liu, X. Zhao, and C. Johnson, "The emerging optical data center" in *Proceedings of OFC/NOEFC '11*, Los Angeles Convention Center, Los Angeles, CA, 2011, OTuH2.
 3. C. Kachris and I. Tomkos, "Power consumption evaluation of hybrid WDM PON networks for data centers," in *Proceedings of the 16th European Conference on Networks and Optical Communication (NOC)*, 2011, 118 – 121.
 4. DatacenterDynamics (DCD) white paper, "The 2011 census," (DCD Industry CENSUS, 2011).
 5. InfiniBand Trade Association, 2012. <http://www.infinibandta.org/index.php>.
 6. Fiber Channel Industry Association, 2012. <http://www.fibrechannel.org/roadmaps>.
 7. H. S. Hamza and J. S. Deogun, "WDM optical interconnects: a balanced design approach," *IEEE/ACM Trans. Netw.* **15**(6), 1565–1578 (2007).
 8. J. Cheng, "Topics in VCSEL-based high-speed WDM optical interconnects," in *IEEE Avionics, Fiber-Optics and Photonics Technology Conference*, 2008, 65–66.
 9. M. Haurylau, G. Chen, H. Chen, J. Zhang, N. A. Nelson, D. H. Albonesi, E. G. Friedman, and P. M. Fauchet, "On-chip optical interconnect roadmap: challenges and critical directions," *IEEE J. Sel. Top. Quantum Electron.* **12**(6), 1699–1705 (2006).
 10. R. Rodes, J. Estaran, B. Li, M. Mueller, J. B. Jensen, T. Gründl, M. Ortsiefer, C. Neumeyr, J. Roskopf, K. J. Larsen, M. Amann, and I. Tafur Monroy, "100 Gb/s single VCSEL data transmission link," in *OFC/NOEFC '12*, OSA Technical Digest (Optical Society of America, 2012), paper PDP5D.10.
 11. L. Chrostowski, C.-H. Chang, R. Stone, and C. J. Chang-Hasnain, "Demonstration of long-wavelength directly modulated VCSEL transmission using SOAs," *IEEE Photon. Technol. Lett.* **14**(9), 1369–1371 (2002).
 12. R. J. Stone, R. F. Nabiev, J. Boucart, W. Yuen, P. Kner, G. S. Li, R. Carico, L. Scheffel, M. Jansen, D. P. Worland, and C. J. Chang-Hasnain, "50 km error-free 10 Gbit/s WDM transmission using directly modulated long-wavelength VCSELs," *Electron. Lett.* **36**(21), 1793–1794 (2000).
 13. FP7 European project GigaWam, "Next-generation WDM-PON enabling gigabit per-user data bandwidth". <http://www.gigawam.org/>.
 14. J. C. Charlier and S. Krüger, "Long-wavelength VCSELs ready to benefit 40/100-GbE modules," *Lightwave®*, 2012. <http://www.lightwaveonline.com/articles/print/volume-28/issue-6/technology/long-wavelength-vcsel-technology-improves.html>.
 15. A. Ran, IEEE P802.3bj 100 Gb/s Backplane and Copper Cable TaskForce 14 January 2012.
 16. F. Chang, K. Onohara, and T. Mizuochoi, "Forward error correction for 100 G transport networks," *IEEE Commun. Mag.* **48**(3), S48–S55 (2010).
-

1. Introduction

Over the past few years, the quick proliferation of Internet use and cloud computing applications has substantially increased the bandwidth needs not only in backbones but prominently in data processing centers (DPCs) [1]. Albeit great part of the traffic will continue to flow between end-users and such computer centers, an increasing fraction is flowing within the DPCs themselves [2, 3]. This situation has triggered a worldwide investment to upgrade the existing facilities or building new ones in order to cope with the growing bandwidth demand that has been estimated to reach \$35BN in 2012 [4]. Accordingly, the major networking technologies for the interconnection of peripherals and data storage keep on releasing roadmaps and future milestones that clearly exceed the 10Gbps barrier, and therefore recently solutions such as fourteen data rate (FDR) of InfiniBand technology [5] or 16GFC of Fiber Channel [6] have been proposed. However, the need to scale to higher and bidirectional transmission capacities (bandwidth milestones reaching 300Gbps by 2013) [5] is also accompanied by the demand to secure high density, low cost, efficiency and reliability.

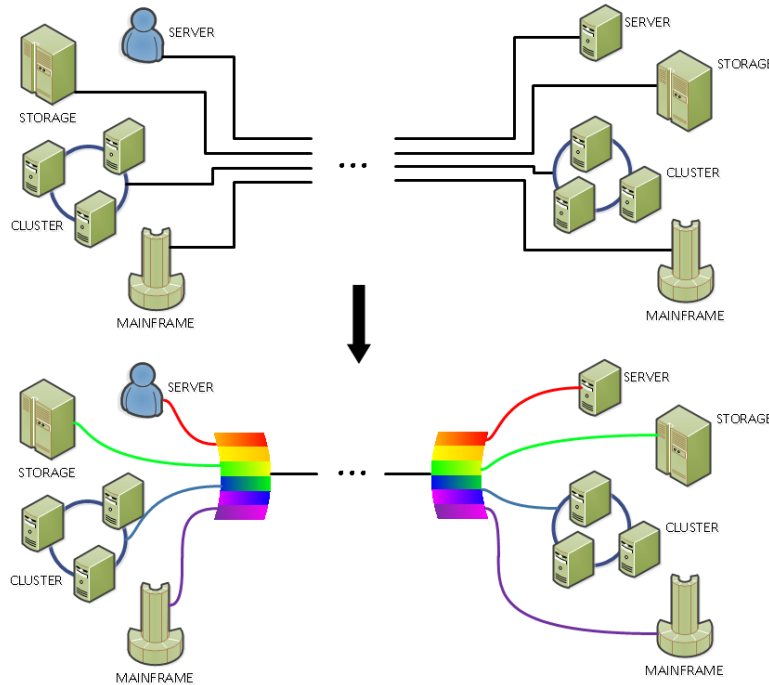


Fig. 1. Datacenter & Storage network topology migration. Multilane/multilink physical point-to-point (P2P) connections (top). L-band VCSEL-based WDM system (bottom).

In this context, wavelength division multiplexing (WDM) techniques in combination with compact integration of light sources and detectors, is an interesting technology candidate for delivering scalable and flexible optical data links with low power consumption, high data throughput, longer transmission distance, and the cost effectiveness needed to efficiently cope with present and future stringent bandwidth requirements in data centers [1, 7–9] See Fig. 1.

In concordance, regarding light sources, VCSELs offer an attractive combination of high bit rates, low power consumption and array integration that along with their tuning capabilities make them perfectly suitable for compact and wideband optical interconnects [8,10].

Long-wavelength technology is relatively new in vertical-cavity surface-emitting lasers (VCSELs). Some investigations [11, 12] have demonstrated the feasibility of long-reach

WDM transmissions at 2.5 Gbps, where L-band is especially suitable due to the lower impact of four-wave mixing (FWM) and the possibility of seizing upon distributed Raman amplification. Some other ongoing investigations are using L-band VCSELs as downstream (OLT to ONU) in a WDM-PON system as the new future proof FTTH technology [13].

In this paper we look into high-speed, cost-efficient and power-efficient VCSEL-based WDM system oriented towards short-range optical fiber connectivity. Four L-band VCSELs are directly modulated with quaternary pulse amplitude modulation (4-PAM) signal at 7 Gbauds to generate a total data nominal rate of 56 Gbps. The multilevel signal has been chosen because of its spectral efficiency,. The 4 lanes are launched into a 50 GHz spaced WDM system. Bit-error rate (BER), crosstalk penalty, transmission penalty and power margin are measured for one of the middle carriers.

The paper is organized as follows. In section 2, a description of the VCSEL used for signal modulation is presented. In section 3, the experimental setup is shown and described. In section 4, details about the digital signal processing (DSP) are provided. Finally, in section 5 the main results and findings are presented.

2. Long-wavelength VCSELs

Historically, VCSELs for longer wavelengths of 1300 to 1700 nm have been difficult to produce because of the refractive index of InGaAsP. But in the early 2000s, development of different combinations of III-V elements led to more practical long-wavelength VCSELs [14]. In general, VCSELs are rapidly becoming the preferable light source for interconnect applications owed to an interesting combination of high modulation bandwidth, low power consumption and reduced manufacturing cost [10]. Besides, their 2-D array integrability, their tuning capabilities and the light coupling ease due to its circular beam, make them perfectly suitable for WDM systems. The following section provides the reader with relevant data about the main characteristics of the device focusing on tunability and temperature considerations.

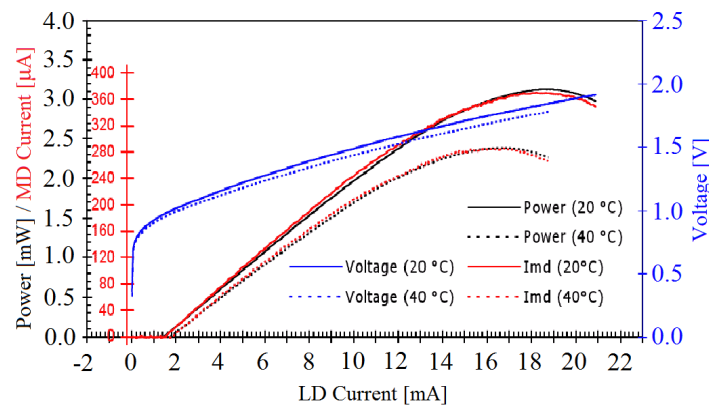


Fig. 2. L-I-V curve of VCSEL#3 and monitor diode (MD) current.

The L-band VCSELs used for the experiments performed in this paper range between 1577 nm and 1583 nm. Such devices exhibit the following measured characteristics: maximum output power around 3 mW and a 3-dB modulation bandwidth of 10 GHz at 20°C. The lasers show fast rise and fall times, low threshold voltage (1.5 mA – 2 mA) with a maximum operating rating around 19 mA, excellent side mode suppression ratio (SMSR) performance and extremely low power dissipation. Figure 2 depicts the L-I-V curve of the VCSEL#3. For its part, VCSELs' tunability depends mainly on bias current and temperature. Table 1 presents concrete measured values about the lasers' tuning ranges at 20°C and 40°C. Figure 3 shows the graphical trend of the emitted wavelength variation with respect to the bias current and temperature for VCSEL#2 (1580.66 nm).

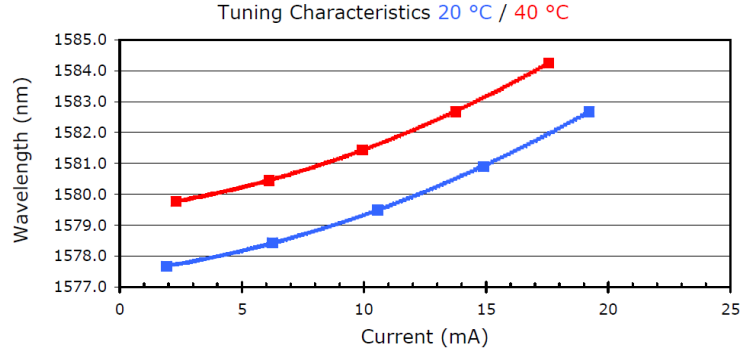


Fig. 3. Tuning characteristics with respect to bias current and temperature of VCSEL#2.

VCSELs are much more sensitive to bias currents concerning wavelength tunability than to temperature. Besides, changing temperature is a slow process, more complicated to control and considerably more power consuming. Thereby, the experiment was conducted inside an isolated room at ambience temperature and the measurements were taken after some stabilization minutes. The impact of the little temperature drifts were corrected through slight variations of the bias currents that never exceeded ± 0.5 mA max. An example of eye diagram correction through bias current is shown in Fig. 4.

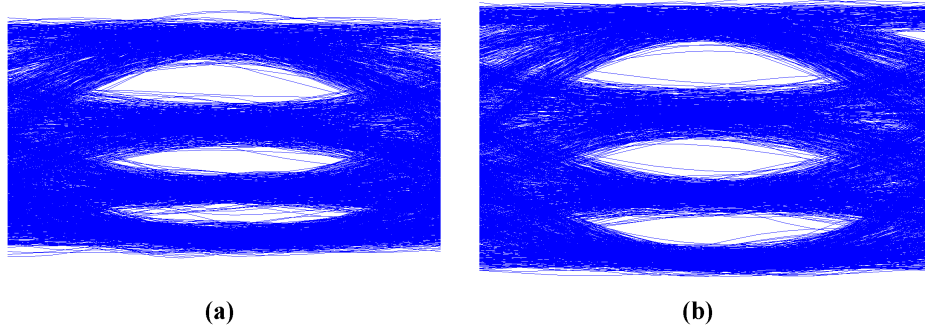


Fig. 4. Illustration of a normalized digital eye diagram before bias current correction (a) and after bias current correction (b).

Table 1. Bias current and their corresponding wavelength interval delimiters for each VCSEL.

	20°C		40°C	
	Bias Current (mA)	Wavelength (nm)	Bias Current (mA)	Wavelength (nm)
VCSEL#1	6.82 / 15.51	1577.87 / 1580.37	6.75 / 14.32	1579.91 / 1582.13
VCSEL#2	6.25 / 14.89	1578.44 / 1580.90	6.12 / 13.75	1580.45 / 1581.44
VCSEL#3	6.23 / 14.48	1579.24 / 1581.90	6.08 / 13.10	1581.24 / 1583.50
VCSEL#4	6.86 / 14.53	1579.97 / 1582.57	6.98 / 13.40	1582.09 / 1584.31

3. Experimental setup

The experimental set-up is presented in Fig. 5. The pulse pattern generator (PPG) is used to generate two pseudorandom binary sequences (PRBS) NRZ streams of length $2^{15}-1$ at 7 Gbps. The 4-PAM electrical signal is generated in the following way: Firstly, the two NRZ streams are passed through 10 dB and 3 dB attenuators respectively in order to reduce reflections and allow us to track the amplitudes while still keeping the convenient proportion for creating the multilevel signal. Time decorrelation matching is adjusted with a mechanical delay-line inserted into the higher power branch. Subsequently, the binary sequences are added up through a 6dB power combiner to make the 14 Gbps 4-PAM signal shown in Fig. 6. The 4-

PAM signal is replicated by four with a 10 GHz active RF splitter. The peak-to-peak voltage after amplification is set to 0.6 V for all the outputs and the time decorrelation between each of them is performed with internal and pre-configured delay lines. The offset of the input signal is tuned to locate the dynamic range well within the most linear range of the internal amplifier.

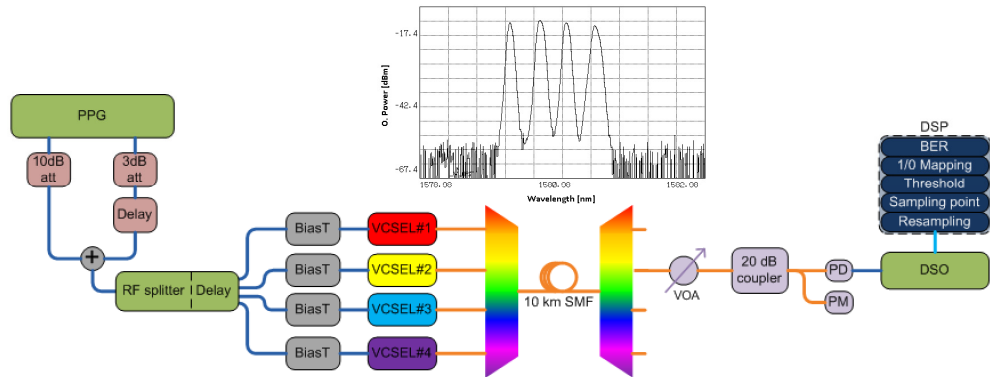


Fig. 5. Experimental setup. Pulse pattern generator (PPG), array waveguide grating (AWG), single mode fiber (SMF), digital storage oscilloscope (DSO), digital signal processing (DSP).

The four outputs of the splitter are driven into the L-band VCSELs. Bias-Ts and evaluation boards are used with an initial bias current of 10.5 mA. The cathode, anode and reference pin of the VCSELs were trimmed off to avoid interferences. Later on, they were appropriately welded to flexible flaps that were connected to the evaluation boards. In order to improve light coupling, four high-precision alignment stations were utilized to approach four independent cleaved fibers to the lasers' aperture. Backwards reflections were drastically reduced by adding index-matching oil to the fibers' end tips. The approaching process was controlled with one microscope and one optical power meter.

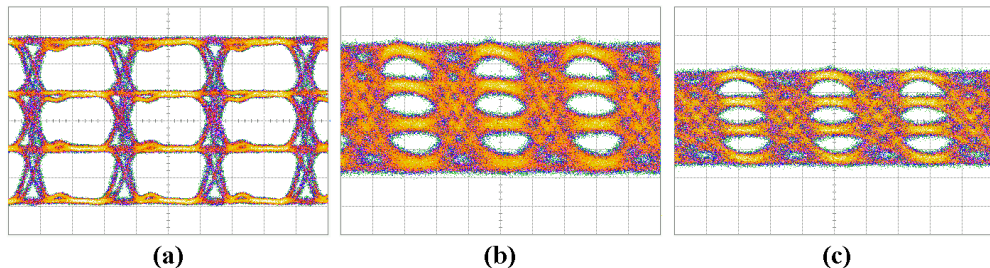


Fig. 6. Electrical 4-PAM signal (a). Optical 4-PAM signal after the VCSEL (b). Electrical 4-PAM after the photodiode (c).

At the optimum light coupling, the lasers showed ~ 2.5 dBm output power for the initial bias current. In this stage the 4-PAM signals were injected (see Fig. 6.). The combined optical spectrum after the first AWG was analyzed. The pre-established 10.5 mA bias currents were tuned independently for each laser to make their output wavelengths match the 50 GHz-spaced AWG's channels. The center wavelengths are 1580.24 nm, 1580.66 nm, 1581.03 nm and 1581.43 nm. Z-axis alignment was modified to create the flat optical spectrum shown in Fig. 5. Minor changes in the bias currents and modulation amplitudes are performed at this stage in order to optimize the individual eye diagrams.

The WDM signal is propagated over a 10 km-long pool of SSMF and demultiplexed with another AWG. At the receiver side, the channel 1580.66 nm is measured. A variable attenuator, a 20dB coupler and an optical power meter are used to control and monitor the incoming optical power. One high-sensitivity PIN photodiode with integrated GaAs

preamplifier and 10GHz of 3-dB bandwidth is used to detect the signal. Finally, a 13 GHz digital storage oscilloscope (DSO) at 40 GS/s is used to store the signal for offline processing.

4. Digital signal processing (DSP)

Quaternary pulse amplitude modulation (4-PAM) is used to achieve 14 Gbps (7 Gbauds) due to the spectral efficiency of 2 bit/s/Hz.. Besides, doubling the modulation frequency in OOK requires more than double power consumption [15]. This section shortly develops on the offline demodulation stages of the 4-PAM signal and the enhancement features of the code to attain improved BER results.

4.1 General BER calculation

For each power level, 10 frames in chunks of $2^{15}-1$ symbols (327670 symbols) are evaluated. Two samples were stored for each power level so that the final BER results are averaged. After storing the signal with the DSO, a ~3-fold up-sampling is performed. This makes around 20 samples per symbol hence allowing the correction of the eye diagram's tilt and facilitating the optimum sampling point calculation. After resampling, reshaping is performed for each of the chunks in order to create a matrix of dimensions 20x327670. This allows us to overlap all the symbols (see Fig. 4.) to calculate the 2-D variance and thereby the optimum sampling point of the combined shapeform.

The histograms for all of the chunks are calculated at the optimum sampling point with 60 bins each. By detecting the bin numbers with the lowest number of observations between peaks, the amplitude thresholds are located. The noise distribution is not taken into account. Once the optimum sampling points are determined, the 1/0 mapping is performed, giving 2 bits for every symbol analyzed (4-PAM). Finally, the BER is calculated by comparing the binary sequences obtained for the least significant bit (LSB) and most significant bit (MSB) with the circularly shifted PRBS used in the signal generation. The exact offset for each bit is calculated by performing x-correlation. When error counting yielded error free transmission, Gaussian fitting and estimated BER was applied. However, its utilization was exclusively necessary to confirm the absence of error floors when the 4 channels were transmitting.

4.2 Enhanced features

Some further advanced signal processing was implemented to improve the BER results. Here we briefly describe three of them. Desynchronization between DSO and our signal, eye diagram tilt correction and Gray coding emulation.

The effect of the desynchronization between the DSO and the signal is a relative displacement of the optimum sampling point with respect to the observation window. If this effect was not taken into consideration, a symbol was counted twice every certain amount of samples. This changes the PRBS offset and consequently increases the BER given that the displacement is only calculated in the very first iteration to reduce the computation time. In order to correct for this, the chunks were in turn subdivided into smaller pieces of around 5000 symbols and the displacement of the sampling point could be tracked with enough precision. When the error occurred, the repeated symbol was automatically deleted and the process continued.

The correction of the eye diagram's tilt literally straightens the eye diagram so that those points with higher variance in every level are put in a common sampling point for the four levels instead of calculating the optimum compromise. An example of this can be observed in Fig. 6 by comparing signal out of the VCSEL and the digitalized one.

Gray coding emulation can be performed when the PRBS is known as well as the relative sequence offset of the LSB with respect to the MSB. In such case, by performing a logical XOR between the original PRBS and itself displaced, a new PRBS is created for the LSB. This reduces the number of errors in the LSB since the mapping for the MSB remains the same.

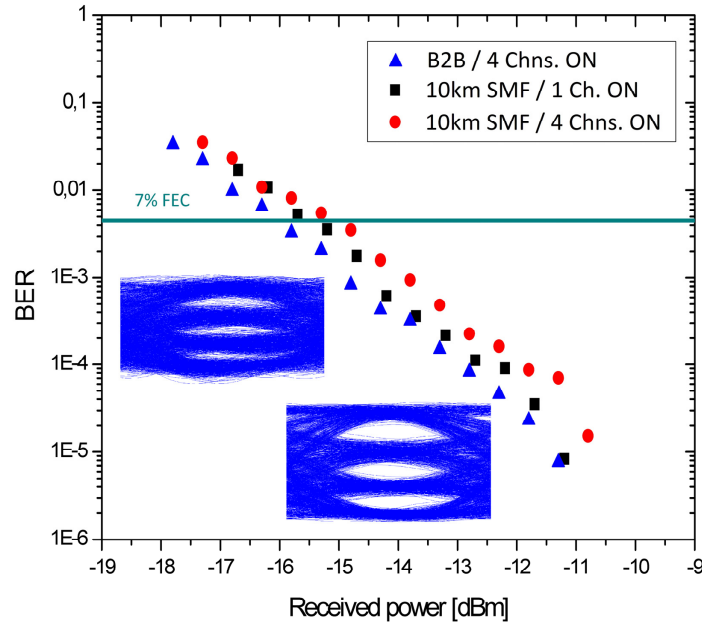


Fig. 7. Averaged BER versus received optical power.

5. Results

The experimental results for each of the three measurements conducted are shown in Fig. 7. Bit error rates are obtained for one of the center channels (1580.66 nm) in back-to-back configuration (blue triangles), after 10 km SMF when only that specific channel is transmitted (black squares) and after 10 km SMF when the four lanes are transmitted in parallel (red circles). Targeting post-FEC bit error rate of 10^{-15} , the green line in Fig. 7 indicates the threshold ($4.5 \cdot 10^{-3}$) [16] of a 7% overhead FEC code.

The BER performance difference between single-channel and four-channel transmission is negligible below ~ 16 dBm received power. For higher power levels, an average crosstalk penalty of less than 0.5 dB is observed. The comparison with back-to-back performance shows a transmission penalty of ~ 0.5 dB with respect to single-lane configuration. Around 1 dB penalty is observed as compared to the four-lane case with a local maximum of 1.3 dB.

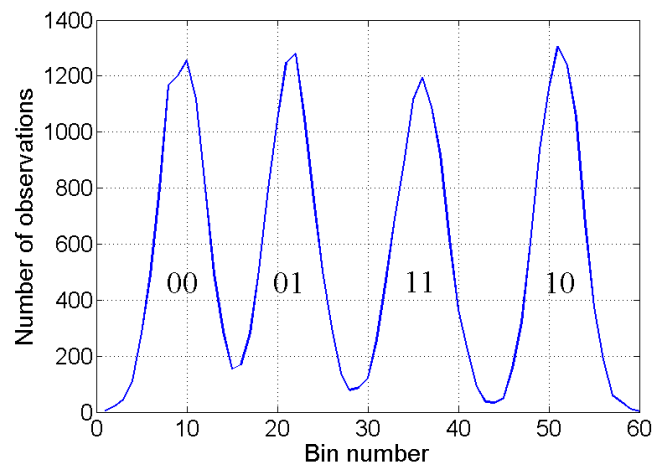


Fig. 8. Histogram of four-channel transmission frame (32767 bits) at -15 dBm.

No error floors are observed within the tested received power interval and the WDM signal clearly exceeds the 7%-FEC threshold for received power levels higher than -15dBm . This grants error free transmission ($\text{BER} \sim 10^{-15}$) under considerably relaxed power budget conditions allowing hence the allocation of $\sim 6\text{-}7\text{ dB}$ extra loss along the link.

Figure 8 shows the received histogram at the optimum sampling point for a frame of $\text{BER} \sim 2.5 \cdot 10^{-3}$ under full WDM operation at the 7%-FEC threshold, which corresponds to -15dBm . Gray mapping is superimposed. The slightly higher accumulation of observations between the 00-01 dip is due to slight instabilities that displace the optimum working point (effect illustrated in Fig. 4.)

6. Conclusions

4x14Gbps L-band VCSEL-based WDM transmission over 10 km of SSMF was investigated. Successful transmission of four channels with quaternary pulse amplitude modulation at 7Gbauds with post-FEC (7% overhead) error free operation has been proven. The crosstalk power penalty was measured to be $\sim 0.5\text{ dB}$ and the power budget margin ranges between 6dB and 7dB. Our results show the potential of the reported system to migrate 4-lanes 56Gbps data links into a compact WDM link.

Acknowledgments

We would like to acknowledge VERTILAS GmbH and Ignis for providing VCSELs and AWGs respectively and the FP7 European project GigaWaM for partly funding this research.